RSC Advances

ROYAL SOCIETY OF CHEMISTRY

www.rsc.org/advances

RSC Advances

COMMUNICATION

Self-assembled fullerene additives for boosting capacity of activated carbon electrodes in supercapacitors

Received 00th January 20xx,
Accepted 00th January 20xx

DOI: 10.1039/x0xx00000x

www.rsc.org/

Deepak Sridhar,[a] Kaushik Balakrishnan,[b] Tony J. Gnanaprakasa,[c] Srini Raghavan[a,c] and Krishna Muralidharan[c*]

Self-assembled fullerene additives at minor weight fractions (~1 wt%) are shown to improve the specific capacity of activated carbon electrodes based supercapacitors significantly, while simultaneously increasing the maximum power density. The integrated approach developed in this work demonstrates the feasibility of using high performance composite carbon electrodes in electrochemical energy storage.

Electrochemical energy storage (EES) devices based on supercapacitors have gained considerable attention due to their superior performance metrics[1–4] (e.g. power density, charge/discharge characteristics, long-term cyclic stability). In particular, supercapacitors employing carbon electrodes have made significant inroads towards commercialization, given the ease of integration of a broad class of carbon electrodes with a variety of electrolytes.[5–13] Among the broad range of carbon structures, activated carbon (AC) is the most widely employed class of electrode materials,[5–7] especially for electric double layer based supercapacitors (EDLC). AC provides good chemical stability and high surface area and can be prepared in large quantities in an inexpensive fashion from petroleum[8,9] and natural[10,11] sources, thereby representing a major focus of research. However, AC is characterized by unevenly distributed pores, as well as a wide distribution of pore sizes, limiting electrolyte accessibility as well as leading to an increase in series and interfacial resistance,[14] which are detrimental to the device performance.[12,13] To alleviate these problems, composites of AC with carbon nanostructures such as graphene-AC[13,15,16] and carbon nanotubes (CNT)-AC[17–19] have been successfully developed, resulting in better control of porosity. Nevertheless, *the more expensive carbon nanostructures are used in comparable proportions* with respect to AC to achieve notable performance improvement. Additionally, conductive polymeric additives such as Nafion,[20] poly [2,5-benzimidazole],[21] poly(3,4-ethylenedioxythiophene)(PEDOT),[22] poly(3- methylthiophene),[23] poly[3-(4-fluorophenyl)thiophene],[24] poly-aniline[25] and many others have also been examined.[26–28] In AC-polymeric additive based electrodes, the net resistance is shown to decrease *though there is a simultaneous decrease in available surface area.*[21,26] Further, the polymeric additives often show pseudocapacitance, but *decrease the cycle-life of the electrode as well the power density.*[29] On the other hand, carbon electrodes that are AC-free and consisting of graphene,[30–32] graphene oxide(GO),[33,34] chemically modified graphene,[35–37] reduced graphene oxide(r-GO),[38–40] carbon nanotubes (CNT)[41–43] have been fabricated, but currently, such electrodes have not yet widely replaced AC based electrodes in commercial supercapacitor systems, due to the elaborate fabrication process.

In this context, we demonstrate for the first time, the ability to significantly improve the capacitive performance of AC-based supercapacitors through the addition of fullerene self-assemblies (FSA),[44] *which constitute only a minor fraction of the electrode-mass*. In this work, the FSA are used in conjunction with electrodes consisting of AC as well as Nafion®, which serves as a binder. The AC used in this work has a relatively low specific area (~ 750 m^2/g).

The FSA considered in this work were synthesized based on a previous investigation, where the ability to control the shape and size of fullerene assemblies on graphene surfaces was demonstrated.[44] The procedure for obtaining FSA is as follows: a solution consisting of C_{60} molecules dissolved in toluene (2mg/ml) was sonicated for two hours and then drop-cast on copper substrates, followed by a directed stream of N_2 at 2 psi for one minute to ensure the removal of toluene. This leads to the rapid self-assembly of FSA within two minutes on copper substrates (which serve as the current collector for the device). More details on the synthesis procedure are given in the Electronic Supplementary Information document (ESI†),

Scanning electron microscopy (SEM) images of FSA that cover the underlying copper surface, are shown in Fig. 1 at different magnifications. The SEM images shown in Fig. 1 typifies the surface coverage across the sample. The FSAs resemble hollow rod-like structures, and their lengths range up to 30 µm. Further, the morphologies of the FSA also vary considerably with some FSA displaying visible cracks as evident in the SEM images The formation of these FSAs can be understood on the basis of nucleation and

[a] *Chemical and Environmental Engineering*
[b] *Collage of Optics*
[c] *Material Science and Engineering*

† Footnotes relating to the title and/or authors should appear here.

Electronic Supplementary Information (ESI) available: [details of any supplementary information available should be included here]. See DOI: 10.1039/x0xx00000x

growth mechanisms as elucidated earlier by Gnanaprakasa et al.[44] Specifically, surface imperfections in copper serve as nucleation sites for adsorbed fullerene molecules, leading to formation of aggregates (i.e. nuclei) at the various surface nucleation sites. Subsequently, during the growth phase, the aggregates grow into larger self-assemblies as a result of diffusion of fullerene molecules within the evaporating toluene film. The resulting open rod-like structures that vary in their size are in contrast to uniform, prismatic nanorods that were formed on graphene on copper substrates as shown by Gnanaprakasa et al.[44]

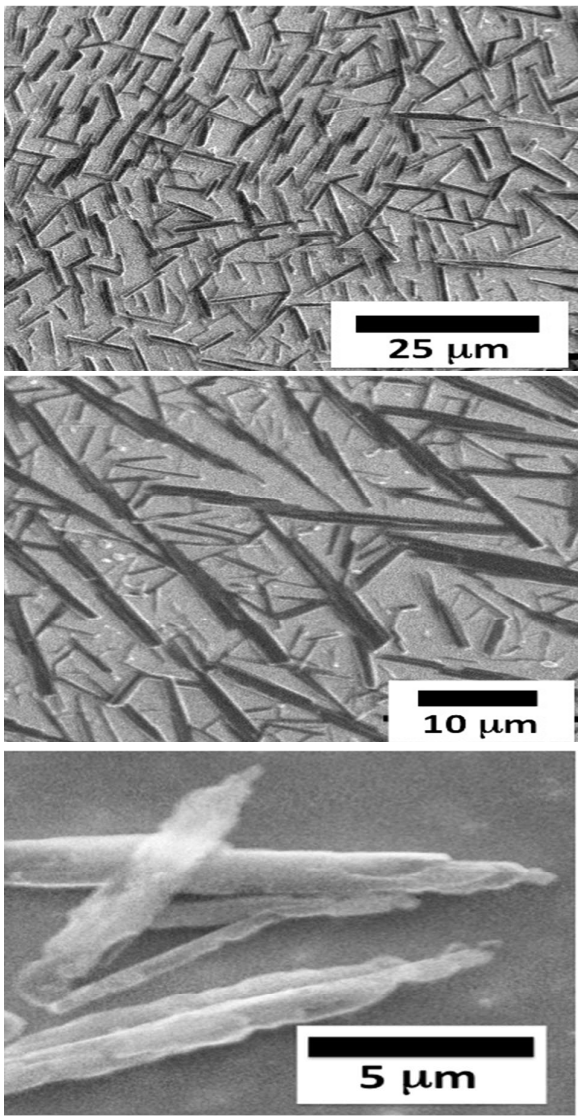

Fig. 1 (a, b, c) Scanning electron microscopy (SEM) images of the FSA on copper obtained at different magnifications

These differences are attributed to the different casting techniques (drop-coating vs dip-coating) as well as the nature of the substrate (copper vs graphene). In particular, graphene grown on copper via chemical vapor deposition is characterized by regular corrugations, which serve as periodic adsorption sites for fullerene molecules. On the other hand, various imperfections such as cold-rolling striations, kinks, jogs, steps and terraces can all be found on copper surfaces. The respective variations in the adsorption sites specific to the graphene (on copper) surface as compared to the plain copper surface underlies the variation in the size and morphology of the FSA on copper as compared to graphene mediated FSA.

The fabrication and analysis protocols for preparing the supercapacitors consist of three steps, namely: (i) electrode preparation using AC, Nafion® and FSA, (ii) supercapacitor assembly using copper, aqueous KOH and cellulose filter sheets (Whatman filter paper grade 1) as current collector, electrolyte and separator respectively and (iii) electrochemical characterization of the supercapacitor performance. Detailed information on the above protocols is given in ESI*.

Two distinct sets of AC-electrodes were prepared in order to examine the performance enhancement of AC based supercapacitors due to FSA addition. The first set of electrodes were devoid of fullerenes and served as the reference system. For clarity and brevity, the samples devoid of FSA are labeled as E-AC, while samples that incorporate FSA are labeled as E-ACC60.

Optical characterization showed that the amount of FSA leading to a high coverage of the underlying copper substrate corresponded to 1-1.2 wt % of the electrode mass of the E-ACC60 systems. In this regard, we chose the lower wt % composition, i.e. 1 wt % FSA for our studies. Also, the structural integrity of the FSA structures was maintained even upon coating with AC and Nafion as shown in ESI† (Fig. S3).

The EDLC fabrication and testing was carried out using established best practices;[45] consequently, electrode thicknesses were ensured to be at least 100 μm and only symmetric two electrode systems were considered. Cyclic voltammetry (CV), electrochemical impedance spectroscopy (EIS) and galvanostatic charge/discharge (CD) were used to examine the performance metrics of the two systems (E-AC and E-ACC60). In addition to the specific capacitance, energy density (E) and maximum power density (P_{max}) were also calculated. The equations employed for the calculations of the performance metrics of the supercapacitors are detailed in ESI†. For each system, a minimum of ten trials were carried out to ensure reproducibility of the materials synthesis and the device fabrication. CV was carried between -0.5 to +0.5 V with scan rates varying from 5-200 mV/s. This operating window was chosen after a series of preliminary tests.

To enable appropriate comparisons between the E-AC and E-ACC60 systems, we first examine the respective CV curves obtained at a scan rate of 20 mV/s as shown in Fig. 2a. Analysis of the CV curves based on ten distinct samples showed that the capacity was highly reproducible with the associated standard deviation equaling (standard deviation?) ± 1 F/g. As evident from Fig. 2a, both curves demonstrate almost ideal rectangular EDLC behavior with the specific capacitance of E-ACC60 (58 F/g) being higher than that of E-AC (43 F/g); this improvement corresponds to approximately 35 % enhancement. This behavior is consistent over different scan-rates as shown in Fig. 2b, the data for which were calculated from the corresponding CV plots for E-AC and E-ACC60 respectively, as given in ESI† (Fig. S4 & S5).

The significant increase in the specific capacitance corresponding to FSA addition can be attributed to the increase in accessible surface area to the electrolyte ions arising due to the morphology and spatial distribution of the FSA structures. Specifically, the rod-like FSA consist of fullerene molecules arranged in a face center cubic (FCC) structure, with the lattice parameter equaling 1.58 nm (see Experimental Section, ESI†). In addition to this underlying micro-porosity of the FSA, additional meso- and macro-porosity is obtained, corresponding to the effective spacing between neighboring FSA that range between few nm to microns as well as due to the open rod-like structures of the FSA. As a result, an increase in the specific capacitance is seen due to FSA incorporation.

In addition to investigating the effect of FSA on specific capacitance, the importance of using FSA on the electrochemical series resistance and interfacial resistance and thereby the power density of the supercapacitors was also studied. To examine this effect, EIS experiments were conducted in the frequency range 10 mHz to 100 KHz and the impedance results were analyzed using the GAMRY G750 software. Specifically, the Nyquist plot impedance data are reported in Fig. 3. The respective impedance curves were fitted to an equivalent circuit (see Fig. S6, ESI†), consisting of (i) an electrochemical series resistance (ESR), (ii) a constant phase element (CPE) representing the capacitance of the system, (iii) an interfacial resistance (Ri) and a (iv) Warburg resistance (W). It is to be noted that this circuit yielded excellent fits for both systems as seen in Fig. S7(ESI†). Importantly, both ESR as well as Ri of the E-ACC60 system was found to be lower than that of E-AC (Table S1, ESI†). The decrease in ESR can be understood in terms of the role of FSA in improving contact between the current collector and electrode. Further, noting that Ri is related to the impedance at the electrode-electrolyte interface[14] as well as the transport of electrolyte ions within the electrode,[46,47] the decrease in Ri of the E-ACC60 system can be attributed to the controlled increase in porosity of the electrode[47,48] due to the presence of FSA. *Thus, the subtle addition of even 1 wt % FSA increases the specific capacitance while reducing the ESR, resulting in the twin enhancement of both energy density (E) and maximum power density (Pmax)* (see Table 1).

The charge-discharge characteristics of the different systems were measured at current densities varying from 0.1 to 0.5 A/g (Fig. S8, ESI†). The capacity measured by the CD measurements at different rates was found to be similar to those measured using CV. Inset of Fig. 4 shows CD curves of the E-ACC60 system at 0.3 A/g. Further, the cyclic stability of both the systems was also tested using the CD experiments and both systems showed excellent cyclic stability. Specifically, both E-AC and E-ACC60 retained 93% of their capacity over 5000 cycles.

To further probe the effect of the FSA, two related studies were undertaken. In the first study, the effect of FSA wt % was examined. It was seen that the specific capacitance increased up to 1 wt %, while the respective specific capacitances at 1 and 1.2 wt % were found to be very similar; beyond 1.2 wt %, the specific capacitance slightly decreased (Fig. S9 ESI*). This observation points to the fact that once the surface coverage is high, the addition of more fullerene molecules does not facilitate the further formation of the rod-like extended FSA structures, which is reflected in the plateauing/slight decrease in the specific capacitance beyond 1.2 wt %.

Next, electrodes that had similar mass and composition as that of the 1 wt % E-ACC60 electrodes were prepared and tested. An important distinction regarding these electrodes is the fact that an equivalent mass (1 wt %) of individual fullerene molecules were simply dispersed within the AC-Nafion mixture which was then cast on the copper substrates. Using CV, the specific capacitance of this system consisting of symmetric electrodes with dispersed fullerenes was evaluated as a function of scan-rate; interestingly, the specific capacitance of this system was always considerably lower than that of the E-AC systems (40 F/g). *This observation unequivocally highlights the role of the FSA on enhancement of AC based supercapacitors.* Specifically, the rod-like, porous FSA provide higher accessible specific area to the electrolytes and improved contact with the current collector, thus enhancing the specific capacitance and other performance metrics such as energy density and maximum power density.

To put our work in context, it is worth discussing other investigations that have reported on fullerene based supercapacitor electrodes. As compared to graphene/GO/r-GO-based and CNT-based supercapacitors, the literature on fullerene as additives is sparse. Relevant literature on fullerene based EDL supercapacitors include Ma et al. (2014)[49] who used fullerenes (10 % by weight) in conjunction with GO, while Okajima et al. (2005)[50] employed AC

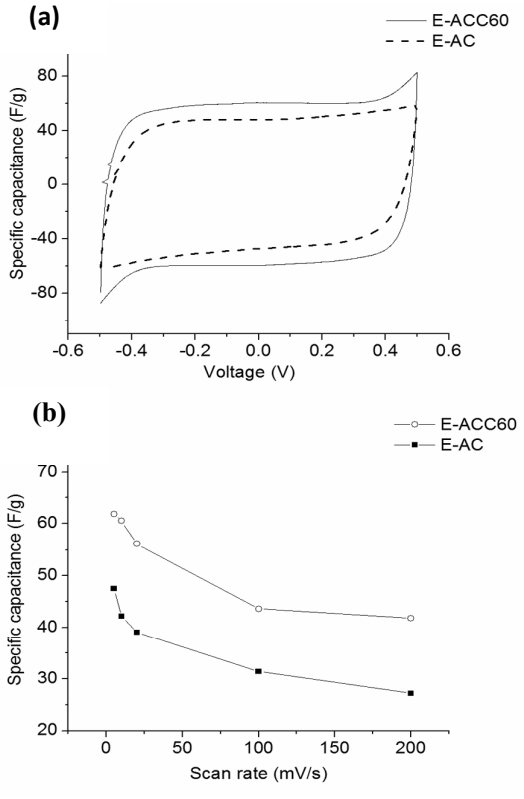

Fig. 2 (a) CV curves of E-AC and E-ACC60 at the scan rate of 20 mV/s **(b)** Specific capacitances of E-AC and E-ACC60 at different scan rates

with fullerenes, with the fullerene fraction ranging up to **30 %** by weight. In both studies, fullerene molecules were simply dispersed within the electrode matrix and no effort was made to either characterize or control the possible self-assemblies of fullerenes.

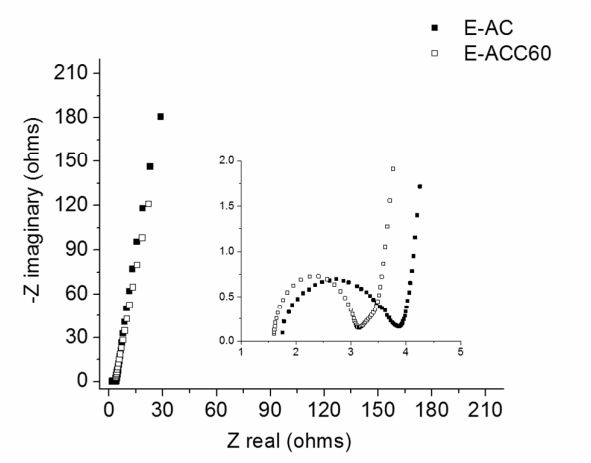

Fig. 3 Comparison of EIS experimental plot along with the values estimated from the model circuit. (Shown within the graph) The inset depicts the enlarged image of the EIS plot at high frequency.

Table 1 Energy density (E) and power density (P_{max}) for E-AC and E-ACC60 electrode systems obtained from CV plots carried out at 20 mV/s.

Electrode	E (Wh/kg)	P_{max} (KW)/kg
E-ACC60	2.2	20.3
E-AC	1.6	17.9

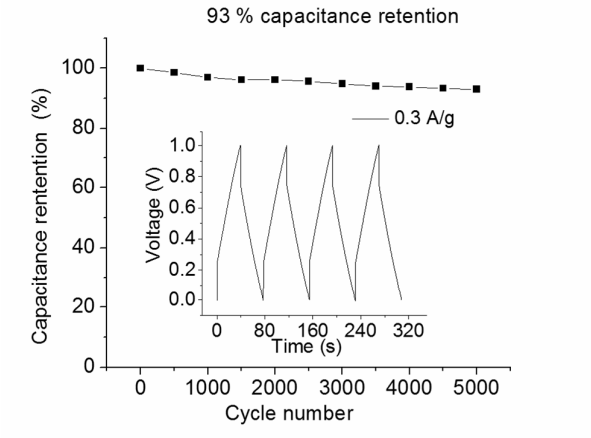

Fig. 4 Cyclic stability of E-ACC60 electrode at 1 A/g over 5000 cycles. (Inset-CD plot for the E-ACC60 system at 0.3 A/g).

Clearly, the distinguishing feature of this work is the fact that we have, for the first time, successfully incorporated fullerene self-assemblies as key constituents in supercapacitors, resulting in a marked impact on performance even at very low weight fractions (1-1.2 wt %). While we have examined FSA in conjunction with relatively low specific area AC, FSA should lead to similar performance enhancement even when they are incorporated with other carbon systems. Further, the procedure developed for electrode synthesis in this work is very simple and straightforward and can be integrated within standard fabrication processes to allow scalable production of high performance low-cost carbon composite electrodes for energy storage applications.

In conclusion, we have demonstrated a simple, facile procedure for improving the performance of AC-based supercapacitors. Specifically, by employing fullerene self-assemblies in conjunction with low-cost activated carbon mixtures, a specific capacitance enhancement of 35% is readily achieved. In addition, other performance metrics such as energy density and maximum performance density have significantly improved along with very good cyclic stability.

Acknowledgements

This work was supported by grants from the Renewable Energy Network at the University of Arizona and GPSC Research-Project Grant Award #RSRCH 103FY'15.

References

1 V. V. N. Obreja, *Phys. E Low-dimensional Syst. Nanostructures*, 2008, **40**, 2596–2605.
2 L. L. Zhang and X. S. Zhao, *Chem. Soc. Rev.*, 2009, **38**, 2520–2531.
3 M. Sevilla and R. Mokaya, *Energy Environ. Sci.*, 2014, **7**, 1250–1280.
4 A. Davies and A. Yu, *Can. J. Chem. Eng.*, 2011, **89**, 1342–1357.
5 E. Frackowiak and F. Béguin, *Carbon N. Y.*, 2001, **39**, 937–950.
6 T. Chen and L. Dai, *Mater. Today*, 2013, **16**, 272–280.
7 A. G. Pandolfo and A. F. Hollenkamp, *J. Power Sources*, 2006, **157**, 11–27.
8 M. Wu, Q. Zha, J. Qiu, X. Han, Y. Guo, Z. Li, A. Yuan and X. Sun, *Fuel*, 2005, **84**, 1992–1997.
9 T. Kawano, M. Kubota, M. S. Onyango, F. Watanabe and H. Matsuda, *Appl. Therm. Eng.*, 2008, **28**, 865–871.
10 M. J. Prauchner and F. Rodríguez-Reinoso, *Microporous Mesoporous Mater.*, 2012, **152**, 163–171.
11 A. L. Cazetta, A. M. M. Vargas, E. M. Nogami, M. H. Kunita, M. R. Guilherme, A. C. Martins, T. L. Silva, J. C. G. Moraes and V. C. Almeida, *Chem. Eng. J.*, 2011, **174**, 117–125.
12 K. H. An, W. S. Kim, Y. S. Park, Y. C. Choi, S. M. Lee, D. C. Chung, D. J. Bae, S. C. Lim and Y. H. Lee, *Adv. Mater.*, 2001, **13**, 497–500.
13 Y. Chen, X. Zhang, H. Zhang, X. Sun, D. Zhang and Y. Ma, *RSC Adv.*, 2012, **2**, 7747.
14 J. Kang, J. Wen, S. H. Jayaram, A. Yu and X. Wang, *Electrochim. Acta*, 2014, **115**, 587–598.
15 C. Zheng, X. Zhou, H. Cao, G. Wang and Z. Liu, *J. Power Sources*, 2014, **258**, 290–296.
16 S. Yu, Y. Li and N. Pan, *RSC Adv.*, 2014, **4**, 48758–48764.
17 G. Xu, C. Zheng, Q. Zhang, J. Huang, M. Zhao, J. Nie, X. Wang and F. Wei, *Nano Res.*, 2011, **4**, 870–881.
18 P.-L. Taberna, G. Chevallier, P. Simon, D. Plée and T. Aubert, *Mater. Res. Bull.*, 2006, **41**, 478–484.

19 B. N. M. Dolah, M. a R. Othman, M. Deraman, N. H. Basri, R. Farma, I. a Talib and M. M. Ishak, *J. Phys. Conf. Ser.*, 2013, **431**, 012015.
20 F. Lufrano, P. Staiti and M. Minutoli, *J. Electrochem. Soc.*, 2004, **151**, A64.
21 R. S. Hastak, P. Sivaraman, D. D. Potphode, K. Shashidhara and a. B. Samui, *Electrochim. Acta*, 2012, **59**, 296–303.
22 T. S. Sonia, P. a Mini, R. Nandhini, K. Sujith, B. Avinash, S. V Nair and K. R. V Subramanian, *Bull. Mater. Sci.*, 2013, **36**, 547–551.
23 A. Balducci, U. Bardi, S. Caporali, M. Mastragostino and F. Soavi, *Electrochem. commun.*, 2004, **6**, 566–570.
24 a. Laforgue, P. Simon, J. F. Fauvarque, M. Mastragostino, F. Soavi, J. F. Sarrau, P. Lailler, M. Conte, E. Rossi and S. Saguatti, *J. Electrochem. Soc.*, 2003, **150**, A645.
25 Q. WANG, J. LI, F. GAO, W. LI, K. WU and X. WANG, *New Carbon Mater.*, 2008, **23**, 275–280.
26 G. Wang, L. Zhang and J. Zhang, *Chem. Soc. Rev.*, 2012, **41**, 797.
27 G. A. Snook, P. Kao and A. S. Best, *J. Power Sources*, 2011, **196**, 1–12.
28 W. Zhang, A. Dehghani-Sanij and R. Blackburn, *J. Mater. Sci.*, 2007, **42**, 3408–3418.
29 M. Mastragostino, C. Arbizzani, L. Meneghello and R. Paraventi, *Adv. Mater.*, 1996, **8**, 331–334.
30 C. Liu, Z. Yu, D. Neff, A. Zhamu and B. Z. Jang, *Nano Lett.*, 2010, **10**, 4863–4868.
31 Y. Bin Tan and J.-M. Lee, *J. Mater. Chem. A*, 2013, **1**, 14814.
32 C. Xu, B. Xu, Y. Gu, Z. Xiong, J. Sun and X. S. Zhao, *Energy Environ. Sci.*, 2013, **6**, 1388.
33 B. Xu, S. Yue, Z. Sui, X. Zhang, S. Hou, G. Cao and Y. Yang, *Energy Environ. Sci.*, 2011, **4**, 2826–2830.
34 N. Li, S. Tang, Y. Dai and X. Meng, *J. Mater. Sci.*, 2014, **49**, 2802–2809.
35 A. K. Mishra and S. Ramaprabhu, *J. Phys. Chem. C*, 2011, **115**, 14006–14013.
36 T. Y. Kim, H. W. Lee, M. Stoller, D. R. Dreyer, C. W. Bielawski, R. S. Ruoff and K. S. Suh, *ACS Nano*, 2011, **5**, 436–442.
37 J. Liu, J. Tang and J. J. Gooding, *J. Mater. Chem.*, 2012, **22**, 12435–12452.
38 Y. Chen, X. Zhang, D. Zhang, P. Yu and Y. Ma, *Carbon N. Y.*, 2011, **49**, 573–580.
39 B. Zhao, P. Liu, Y. Jiang, D. Pan, H. Tao, J. Song, T. Fang and W. Xu, *J. Power Sources*, 2012, **198**, 423–427.
40 X.-Y. Peng, X.-X. Liu, D. Diamond and K. T. Lau, *Carbon N. Y.*, 2011, **49**, 3488–3496.
41 M. Endo, Y. J. Kim, T. Chino, O. Shinya, Y. Matsuzawa, H. Suezaki, K. Tantrakarn and M. S. Dresselhaus, *Appl. Phys. A Mater. Sci. Process.*, 2006, **82**, 559–565.
42 B. Kim, H. Chung and W. Kim, *Nanotechnology*, 2012, **23**, 155401.
43 W. Lu, L. Qu, K. Henry and L. Dai, *J. Power Sources*, 2009, **189**, 1270–1277.
44 T. J. Gnanaprakasa, D. Sridhar, W. J. Beck, K. Runge, B. G. Potter, T. J. Zega, P. A. Deymier, S. Raghavan and K. Muralidharan, *Chem. Commun.*, 2015, **51**, 1858–1861.
45 M. D. Stoller and R. S. Ruoff, *Energy Environ. Sci.*, 2010, **3**, 1294.
46 X. Xia, Q. Ma, S. Yi, H. Chen, H. Liu, Y. Chen and L. Yang, *Mater. Chem. Phys.*, 2014, **148**, 631–638.
47 K. Tõnurist, I. Vaas, T. Thomberg, A. Jänes, H. Kurig, T. Romann and E. Lust, *Electrochim. Acta*, 2014, **119**, 72–77.
48 D. Wu, X. Chen, S. Lu, Y. Liang, F. Xu and R. Fu, *Microporous Mesoporous Mater.*, 2010, **131**, 261–264.
49 J. Ma, Q. Guo, H.-L. Gao and X. Qin, *Fullerenes, Nanotub. Carbon Nanostructures*, 2014, **23**, 477–482.
50 K. Okajima, A. Ikeda, K. Kamoshita and M. Sudoh, *Electrochim. Acta*, 2005, **51**, 972–977.